buildings

MDPI

Article

Everyday-Carry Equipment Mapping: A Portable and Low-Cost Method for 3D Digital Documentation of Architectural Heritage by Integrated iPhone and Microdrone

Nan Zhang [1,2] and Xijian Lan [1,*]

[1] School of Architecture, Tianjin Chengjian University, Tianjin 300384, China; zhangnan@tcu.edu.cn
[2] School of Civil Engineering, Tianjin University, Tianjin 300350, China
* Correspondence: fllxjhhh@163.com

Abstract: Mapping constitutes a critical component of architectural heritage research, providing the groundwork for both conservation and utilization efforts. Three-dimensional (3D) digital documentation represents a prominent form of mapping in the contemporary era, and its value is widely recognized. However, cost and portability constraints often limit its widespread use in routine research and conservation initiatives. This study proposes a cost-effective and portable approach to 3D digital documentation, employing everyday-carry (EDC) equipment, the iPhone 15 Pro and DJI Mini 4 Pro, for data acquisition in architectural heritage. The workflow was subsequently optimized, and the datasets from the iPhone-LiDAR and microdrone were seamlessly integrated, resulting in an integrated 3D digital model of both the indoor and outdoor spaces of the architectural heritage site. The model demonstrated an overall relative error of 4.93%, achieving centimeter-level accuracy, precise spatial alignment between indoor and outdoor sections, clear and smooth texture mapping, high visibility, and suitability for digital display applications. This optimized workflow leverages the strengths of both EDC equipment types while addressing the limitations identified in prior studies.

Keywords: everyday-carry (EDC); point cloud; structure-from-motion (SfM) photogrammetry; 3D reconstruction; iPhone-LiDAR scanning

check for updates

Academic Editor: Grzegorz Ludwik Golewski

Received: 26 November 2024
Revised: 19 December 2024
Accepted: 24 December 2024
Published: 30 December 2024

Citation: Zhang, N.; Lan, X. Everyday-Carry Equipment Mapping: A Portable and Low-Cost Method for 3D Digital Documentation of Architectural Heritage by Integrated iPhone and Microdrone. *Buildings* **2025**, *15*, 89. https://doi.org/10.3390/buildings15010089

Copyright: © 2024 by the authors. Licensee MDPI, Basel, Switzerland. This article is an open access article distributed under the terms and conditions of the Creative Commons Attribution (CC BY) license (https://creativecommons.org/licenses/by/4.0/).

1. Introduction

Architectural heritage faces a variety of environmental challenges and the possibility of destruction, so digital documentation can prove an effective tool for the protection, regulation, and risk prediction associated with these buildings [1,2]. In the past, architectural heritage was documented in two-dimension (2D) using tools such as paper, pen, and tape measures. Recently, non-intrusive three-dimensional (3D) digital documentation has become an essential method for archiving [3,4], and in some cases, a standard practice in architectural heritage [5,6]. These 3D reconstructions provide enhanced opportunities for education, research, conservation, and management [7–9]. For example, 3D digital documentation can be utilized in academic institutions to overcome spatial limitations, enabling more comprehensive architectural heritage research [10]. It can also serve as a data foundation for relevant departments in managing architectural heritage [9]. After the demolition of a building, the 3D digital record could serve as a crucial testament to its existence and provide a foundation for reconstruction efforts [1,11].

The choice of method for heritage documentation should depend on the desired outcomes and the feasibility of the approach. The scale of architectural heritage typically

exceeds that of the human body. Consequently, it is often necessary to integrate both range-based and image-based techniques to obtain a more comprehensive digital representation of buildings [12–15]. The prevailing methodology typically involves the use of terrestrial laser scanners (TLSs) in conjunction with professional mapping drones (PMDs) to generate millimeter-level documentation and complete studies such as structural simulation [16] and damage estimation [17]; TLSs are commonly used to collect data from the interiors of buildings. To obtain surface data of geometric objects, active sensors that emit and receive laser beams are used [18]. The use of PMDs facilitates the acquisition of images from areas inaccessible to ground-based laser beams such as roofs and other blind spots. Additionally, it captures the surrounding landscape of architectural heritage in a short time. The PMD image dataset, with sufficiently high overlap, is acquired and subsequently reconstructed using structure-from-motion (SfM) photogrammetry software to generate 3D data [19,20]. Ultimately, the two datasets are integrated into a single coordinate system to create a comprehensive 3D documentation of architectural heritage [21]. Nevertheless, four issues are inherent to this conventional approach:

1. High-cost: The financial investment required for TLSs exceeds 50,000 USD, while PMDs have a minimum cost of 10,000 USD. These costs are beyond the means of most architectural heritage conservation groups and academic institutions [22,23]. The financial constraints associated with architectural heritage preservation often also lead to delays [24].
2. Insufficient portability: The combined weight of the TLS, mapping drone, and their respective protective cases exceeds 15 kg, posing a challenge to the operators' endurance at heritage sites that can only be accessed on foot.
3. Regulatory restrictions: PMDs face challenges in securing funding, meeting pilot skill requirements, and obtaining take-off permits and flight licenses [25].
4. Poor visibility: The varying sources of 3D data colorization for TLSs and drones result in biased color representations of the same area. High-resolution textures that preserve visual information [8,19] are as equally important as geometric accuracy in heritage research [5,15].

The relentless pursuit of mapping precision may not always be the most prudent approach in architectural heritage conservation [26]. Researchers must often balance the accuracy of their findings with the feasibility of their methods. Low-cost, portable equipment can often be an effective means of achieving the desired outcomes. As technology advances, equipment capabilities improve and costs decrease, thereby broadening access to architectural heritage information in various contexts.

As demonstrated by [24], low-cost research on 3D mapping sensors has shown a growing trend over the past five years, with sensor technology becoming more integrated and affordable. In architectural heritage, the use of consumer drones (e.g., DJI's Phantom) in combination with digital SfM photogrammetry to create 3D models has emerged as a cost-effective alternative [27,28]. However, despite being more affordable than PMDs, the cost and weight of the drones used in this methodology remain considerable, and the resulting models are limited to outdoor environments excluding indoor spaces.

Over the past few decades, scanning technology has significantly decreased in cost and has diversified, evolving from expensive tripod-mounted laser scanners to backpack systems, handheld devices, and more recently, the integration of sensors into smart devices [24,29] such as Microsoft Kinect (2010) [30] and Google Tango (2014) [31]. However, this type of equipment has not gained widespread adoption as a low-cost alternative due to the unsatisfactory quality of the results it produces [20].

In 2020, Apple Inc. introduced highly integrated, miniaturized LiDAR sensors in its Pro line of iPhones and iPads [32], bringing LiDAR technology into everyday-carry (EDC)

devices. Over four years of development, iOS applications integrating scanning technology have provided expanded for mapping [24]. The iOS-LiDAR (i.e., iPhone-LiDAR and iPad-LiDAR) devices have the potential to engage non-experts in the digital 3D documentation of architectural heritage [23], primarily because these ubiquitous tools are already familiar to the public.

Furthermore, technological advances have incorporated features originally exclusive to PMDs into consumer-grade models. The introduction of more rigorous regulations has driven the development of compact drones, such as DJI's Mini series, which maintain a take-off weight under 250 g while providing high-precision photographic and positioning capabilities. Their lighter weight allows them to bypass the user qualification requirements of most drone flight regulations [33], making them more portable and broadening their range of applications. These microdrones are widely regarded as excellent EDC aerial photography tools by photography enthusiasts. These low-cost, portable EDC devices can therefore facilitate more extensive digital documentation of architectural heritage.

The use of EDC equipment, as outlined previously, enables the capture of 3D data from architectural heritage. This approach can address the first three issues outlined earlier (the cost, portability, and restrictions); however, it should be noted that the accuracy of the data may be reduced compared to that obtained with professional-grade equipment.

This study aimed to develop a reproducible, cost-effective, and portable 3D digital documentation method for architectural heritage using iPhone-LiDAR and a microdrone. It also involved assessing the precision of the 3D models generated by this workflow and presents a potential solution to the fourth issue above-mentioned (poor visibility). Concurrently, this method addresses several issues associated with existing low-cost 3D documentation approaches such as the lack of indoor spaces in the resulting models and suboptimal result quality.

2. Reliability of EDC Equipment

Apple's ARKit enables the rapid generation of high-resolution 3D digital models [26,34,35] using integrated iOS device sensors [36,37], such as LiDAR and the inertial measurement unit (IMU), and operates similarly to simultaneous localization and mapping (SLAM). This provides a comfortable and interactive scanning experience, allowing users to view the process in real-time [38] and make immediate adjustments to unscanned elements. Additionally, their compact size and lightweight design have enhanced their popularity both among researchers and the general public.

Recent research has demonstrated that the precision and accuracy of iOS-LiDAR devices can be applied across various fields including forestry [22,23,39], geology [32,40,41], and criminology [42]. These devices can map real-world features and generate digital models with an accuracy of up to 10 cm [22,29,36]. Several researchers have mounted iPhones on commercial drones [43] and scooters [44] to adapt them for research purposes. Some scholars have integrated iPhone scanning data with drone-captured data, as demonstrated in [45], where a large reconstruction model was used to locate a sinkhole using drone data, while a field survey reconstructed a model of the crater with an iPhone. In [46], the iPhone's high oblique angle was used to collect point cloud data of a building's structure, which was subsequently integrated with aerial data.

The iOS-LiDAR devices are equipped with a high-resolution camera system, enabling the reconstruction of models through precise mapping. This facilitates the restoration of scene details during post-processing, offering a superior alternative to traditional TLS equipment. This is particularly beneficial in the field of heritage preservation. Additionally, several experts in archaeology and history have used iOS-LiDAR devices for the digital documentation of movable cultural heritage [37,38,47] and archaeological site records [48].

Architectural historians have also employed them for the reconstruction of the indoor spaces in ancient temples [49].

The scanning and reconstruction capabilities, along with integrated high geometric accuracy, fast processing speed, low cost, and high resolution [34], indicate that iOS-LiDAR devices have significant potential for future applications in cultural heritage and other disciplines [38,49]. Moreover, iOS-LiDAR devices have been utilized for scanning indoor spaces. By comparing the point cloud data with those obtained via TLSs, it has been shown that iOS-LiDAR devices can achieve an accuracy within 7 cm [29,36,50,51]. However, it has been observed that as the scanning time increases, the resulting point cloud data may exhibit drift errors and texture mapping mismatches [35,36,52]. Therefore, iOS-LiDAR devices are better suited for small-scale spatial mapping [29,35].

The use of microdrones for mapping is not a novel phenomenon [25,28,33]. Weighing less than 250 g, such as the DJI Mini 2, microdrones have been validated as replacements for commercial drones when combined with ground control points (GCPs) for geographic alignment. These have even been shown to reconstruct 3D digital models of higher quality than those produced by the DJI Phantom 4 Pro V2 [53]. The combination of low-cost, lightweight design, and small size makes them an ideal solution for field mapping in the cultural heritage sector, particularly when working with a limited budget [54]. Additionally, the lightweight construction of microdrones helps keep the damage to an acceptable level, reducing the risk of harm to heritage sites in the event of a collision. However, the camera integrated into the microdrone must be sufficiently advanced to meet the requirements of mapping. Therefore, it is not advisable to use microdrones with lower-quality cameras for mapping tasks [55].

3. Datasets Preparation

3.1. Study Site

This study was conducted at the 'Shuangmei Mansion' (hereafter referred to as the Mansion), located in Xiaolan Town, Zhongshan City, Guangdong Province, China. The building was constructed in the 1940s as a private residence and was later converted into a folklore museum in 2011 and upgraded in 2023 to an intangible cultural heritage exhibition hall, with its original layout preserved. As shown in Figure 1, the Mansion's architectural style reflects a synthesis of Chinese and Western influences. The interior consists of six spaces, each furnished with physical and graphic displays of Xiaolan Town's intangible cultural heritage.

The Mansion was selected as a case study for its broad applicability, characterized by its medium size and decorative motifs that reflect its historical character, despite not being particularly old or historically significant. It features Chinese-style roofs and Western-style corridors, exemplifying the convergence of Chinese and Western architectural traditions. This type of architectural heritage may not require significant manpower or resources for detailed mapping or high-precision results. However, ensuring its preservation and digital documentation in accordance with contemporary standards is crucial.



Figure 1. Study site condition of 'Shuangmei Mansion'.

3.2. Selection of EDC Equipment

The results of LiDAR scanning conducted on both an iPhone and iPad were largely found to be similar [32]. In this study, scanning was performed using an iPhone 15 Pro, selected for its portability and employed for indoor scanning. The device uses the time-of-flight (ToF) method with the SPAD Sony IMX591 LiDAR sensor, which has a resolution of 0.01 megapixels and a pixel pitch of 10.1 microns [41]. The sensor works by measuring the travel time of laser beams through emission and reflection to obtain the spatial coordinates of an object's surface at distances of up to 5 m.

Previous studies [19,34,52] have shown that using a photographic gimbal during iPhone-LiDAR scanning can effectively mitigate the negative effects caused by abrupt movements of the IMU sensor. In this experiment, the DJI Osmo Mobile 6, a 3-axis gimbal, was chosen for each scan due to its collapsible design, making it space-efficient.

The DJI Mini 4 Pro was used to capture images of the Mansion's outdoor spaces. Following four generations of DJI mini drones, the Mini 4 Pro features a larger sensor (1/1.3″) and a higher resolution (48 MP), allowing it to capture the Mansion's color and detail accurately. Its compact size and 249 g weight facilitate smooth take-offs and operation across various flight zones, while the 6-direction sensors enhance safety. Additionally, its affordable price of 1099 USD makes it accessible to students and non-professional users. The integration of a global navigation satellite system (GNSS) and an IMU sensor allows for direct georeferencing, enabling the measurement of the camera's geographic real-time position during flight.

The full specifications of the EDC equipment including a total weight of 1475 g and a price of 2237 USD are provided in Figure 2.



Figure 2. EDC equipment used in this study.

3.3. Obtaining Datasets

In this study, the 3D Scanner App (version 2.1.3) was selected for indoor scanning. Compared to other scanning applications, its algorithm effectively filters noise, resulting in residuals with a normal distribution and more homogeneous spatial distribution [35]. Additionally, it allows for the free export of the digital model in multiple formats. During the acquisition process, the 3D Scanner App captures low-resolution (2.7 MP) images at a frequency of approximately 2 Hz, primarily for generating texture maps and assigning RGB attributes to the point cloud. These images can also serve as a backup dataset, allowing researchers to retrace the heritage site in future work.

According to the experiments in [56], the scanning distance range for the iPhone-LiDAR was found to be between 0.3 and 2 m from the geometric object. In this study, however, the indoor scanning distance was maintained within the range of 0.5 to 1.5 m, with the iPhone held upright to ensure the visibility of the front of the LiDAR sensor.

The Mansion contains six indoor spaces, each scanned using a 'wrap-around' acquisition method, as indicated by the blue line in Figure 3. The spaces were scanned independently to minimize drift errors resulting from the scanning time [52]. The six generated indoor point cloud models, with high density, were exported in *.las format, along with the scanned texture mapping source image dataset.

Note that the iPhone was unable to receive a strong GPS signal indoors, which affected the accuracy of the generated model. In this study, the 'GPS' option was deactivated, and the geographic data obtained from the microdrone were used to assign a spatial coordinate axis to this section of the model during subsequent processing (Section 4.2).

The DJI Mini 4 Pro was used to capture images of the roof and the building's façade from three perspectives, as shown in Figure 4: vertically, obliquely, and close-range. To achieve vertical and oblique photography, the flight altitude was maintained at 30 m, utilizing flight planning and circling maneuvers. For close-range photography, 'lateral movements to the left and right' were performed. However, to capture the front and rear of the main façade, within 2 m of the decorative features, further detailed images were needed. Manual flights were conducted in sheltered areas to avoid obstacles and ensure complete image data collection. Regardless of the methodology used to capture the images, it was imperative to ensure an overlap range of 70% to 80%. The final outdoor dataset consisted of 852 images.

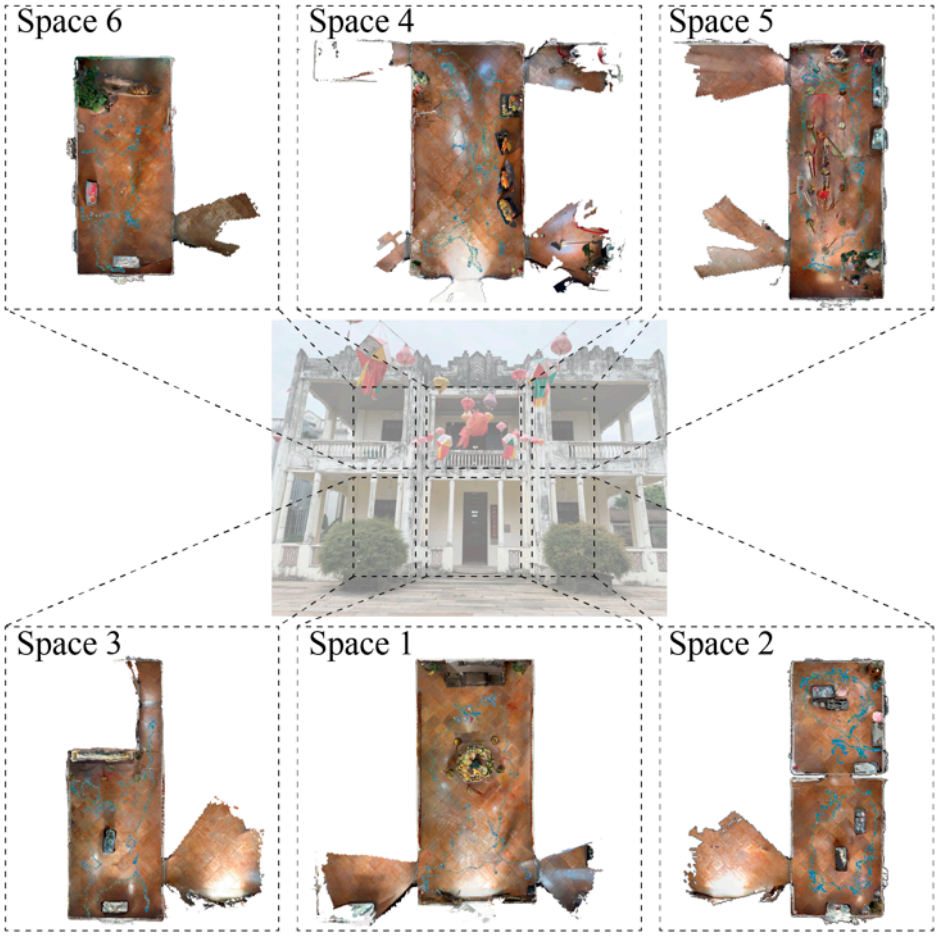


Figure 3. 'Wrap-around' acquisition method for six indoor spaces using iPhone-LiDAR scanning (the blue line in each space is the path of the scan.).

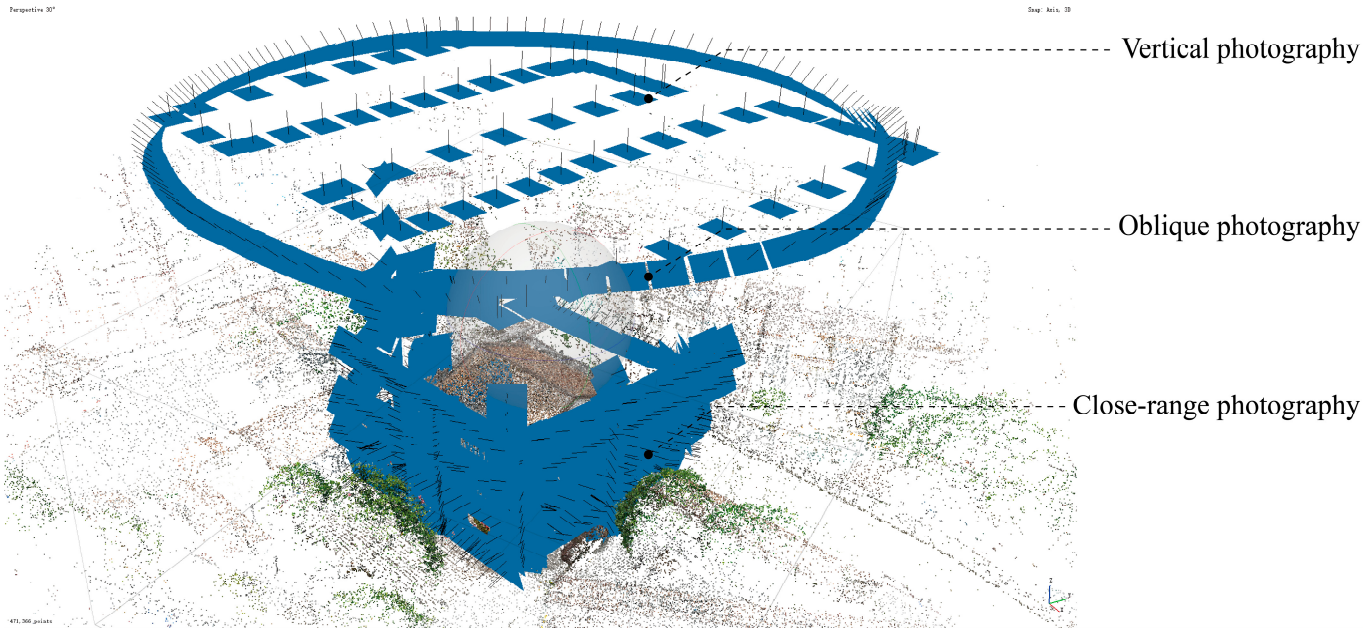


Figure 4. Camera positions for microdrone data acquisition using the DJI Mini 4 Pro.

Changes in light and shadow during data collection may impact the results. Therefore, it is advisable to choose cloudy days for data collection and to conduct the process quickly using the microdrone.

4. Optimal Workflow to Integrate Both Data

The three datasets obtained in accordance with Section 3.3 are as follows:

1. Outdoor images captured by the DJI Mini 4 Pro;
2. Texture source images captured by the iPhone 15 Pro using the 3D Scanner App;
3. Six point cloud models exported from the 3D Scanner App.

The following section provides a detailed overview of the optimization work conducted in this paper, starting with an introduction to the underlying theories (Section 4.1), followed by a description of the specific operations employed (Section 4.2).

4.1. Theories

An important step was to perform a 3D reconstruction using Agisoft Metashape Pro (version 2.1.1), which employs SfM photogrammetry, to generate a 3D digital model of the Mansion. This process was carried out in several steps: after importing the images, the software automatically performs the reconstruction workflow, which involves aligning images, georeferencing, generating the dense point cloud, reconstructing mesh surfaces, refining the mesh, and mapping textures from the original images.

Considering the existing knowledge and applications of artifacts and remote sensing, architectural heritage, due to its substantially larger scale compared to movable artifacts, requires a distinct approach. Unlike the model replacement and texture mapping techniques discussed in [5,8], replacing the mesh model of an entire building typically requires the use of aerial laser scanner (ALS) data. However, this approach is not practical due to the limited budgets available in the field of architectural heritage [24]. Given the available data, replacing the indoor model is feasible. In summary, the optimal method involves replacing the indoor model using digital SfM photogrammetry, with the indoor model exported from the iPhone-LiDAR, followed by mesh rebuilding and texture remapping.

Registration to a common coordinate system ensured a relatively close alignment of both models. For this purpose, the open-source software CloudCompare (version 2.13) was employed. Initially, 'same points matching' was used to align the models of the two parts. Subsequently, precise registration of the two models was achieved using the iterative closest point (ICP) algorithm, which involves searching for pairs of nearest adjacent points in the two datasets and calculating the transformation parameters between them [18].

4.2. Operational Details

Replacing the indoor point cloud is a crucial step in the optimization process, which must be completed before the mesh reconstruction stages. The precise replacement of the point cloud data was performed in CloudCompare, and subsequently, the integrated mesh model was generated from the replaced point cloud data and texture remapping using the aligned image dataset in Metashape Pro.

The following section describes the optimization workflow, with the detailed step-by-step process illustrated in Figure 5.

1. The outdoor image dataset from the DJI Mini 4 Pro was imported into Metashape Pro, where effective alignment achieved a recognition rate of 99.89% (with the accuracy set to 'Highest' and the options 'Generic preselection' and 'Reference preselection' selected), generating a tie points model. No additional GCPs were set up in this study to lower the learning threshold for beginners and amateur practitioners. Only micro-

drone photographs with geolocation data were used to create a tie point model based on the microdrone's onboard GPS data in the WGS84 geographic coordinate system.

2. The indoor images of the scanned texture source data exported from the 3D Scanner App were manually filtered for quality. Given the large number of images exported from the dataset, it is evident that excessive overlap will increase the software processing time. Additionally, images blurred by sudden movements during scanning may compromise model accuracy.
3. The filtered indoor images from Step 2 were then imported into a newly created chunk in Metashape Pro, where a scaled tie point model was generated after photo alignment. Six new chunks were created independently for the Mansion's six indoor spaces, with the corresponding images imported. At this stage, each tie points model was automatically assigned a local coordinate system by the software. Additionally, the alignment results were not unique and can be refined through multiple alignments to achieve more accurate tie point results.
4. Six indoor chunks from Step 3 were aligned with the outdoor chunk in Metashape Pro. A minimum of three common points must be marked in the images to align each chunk. The alignment of the chunks required using the outdoor chunk with the WGS84 coordinate system as the 'reference', enabling the accurate 'shift' of the indoor chunk from the local scaled coordinate system to the WGS84 geographic coordinate system.
5. The chunks were merged into a new chunk, and the options to 'merge tie points' and 'merge images' were selected. A 'High-Quality' point cloud model was then generated and exported in *.las format.

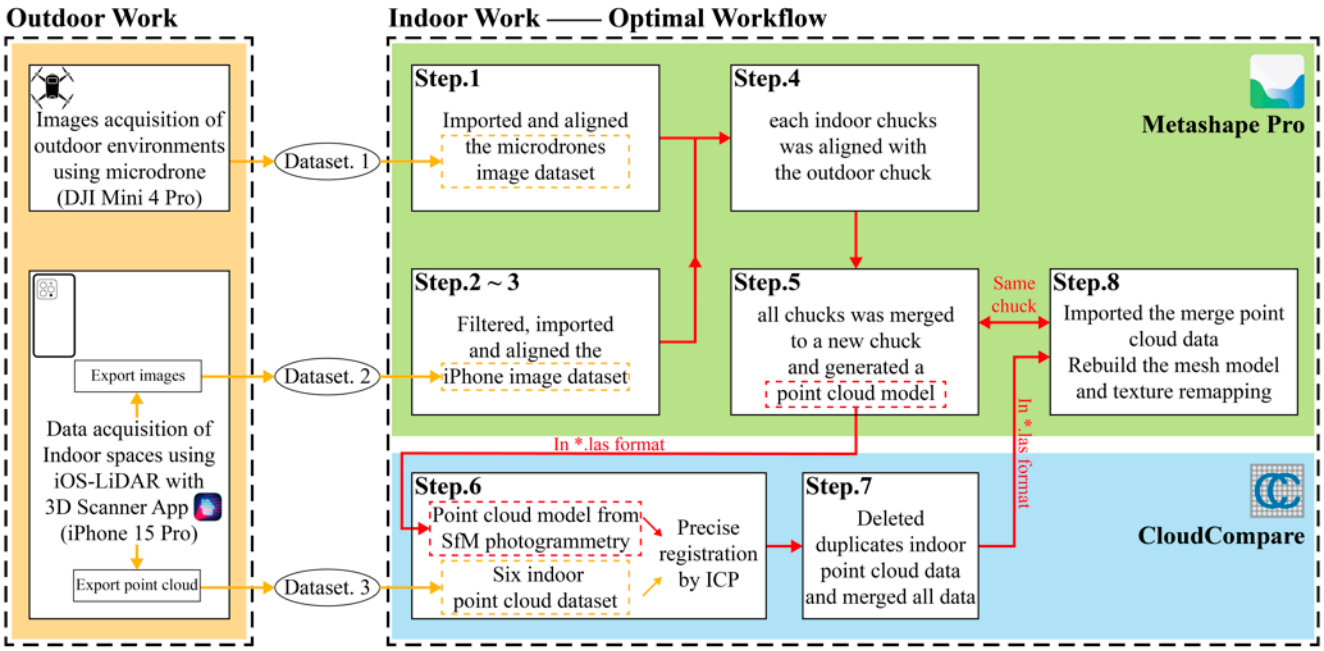


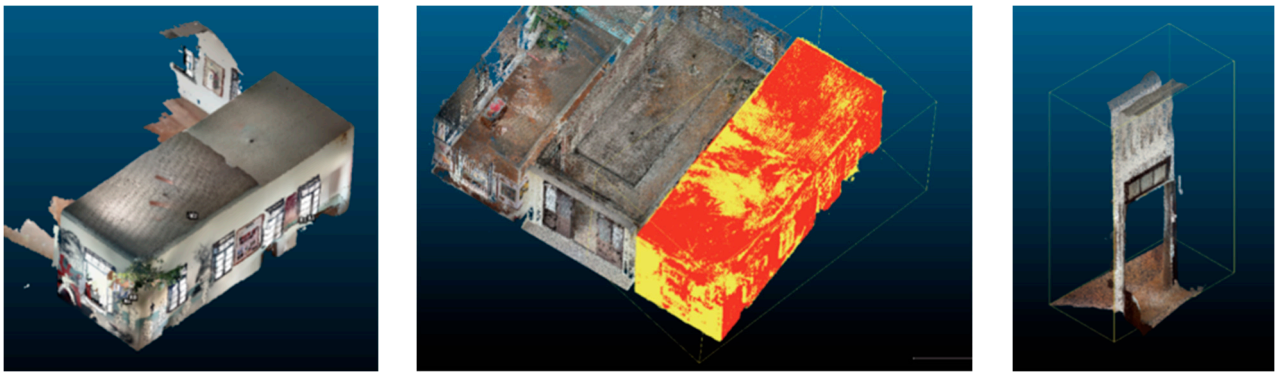
Figure 5. Step-by-step workflow optimization approach.

In the first five steps, the Mansion's 3D point cloud model, incorporating both indoor and outdoor spaces, was created in Metashape Pro using two image datasets (datasets 1 and 2) via digital SfM photogrammetry. Subsequently, the six indoor point cloud models were replaced with the iPhone-exported point cloud data (dataset 3).

6. Each model exported from the 3D Scanner App and Step 5 was imported into CloudCompare for model alignment and ICP registration, as shown in (a) and (b) of Figure 6. The point cloud exported from Step 5 should be used as the 'reference' model to ensure

that the coordinates remain unaltered. Additionally, the 'adjust scale' option should be selected when using the ICP registration. To simplify the process, each indoor space was treated independently in this study.

7. The duplicate indoor data from the SfM photogrammetry were removed, and the remaining point clouds were merged into a single file, which was then exported in *.las format. The intersection between the replaced and original point clouds, is shown in (c) of Figure 6.
8. The merged point cloud was imported into the chunk created in Step 5 in Metashape Pro to rebuild the mesh model and perform texture remapping using the aligned images. The final mesh model was exported in *.obj format. In this study, the 'High-Quality' and 'Medium-Face Count' options were selected to rebuild the mesh model, and the 'Images-Source Data' option was selected for texture remapping.



(**a**) (**b**) (**c**)

Figure 6. Optimized workflow in CloudCompare: (**a**) point cloud alignment using 'same points matching'; (**b**) accurate point cloud registration using the ICP algorithm; (**c**) handling intersections between the replaced and original point clouds.

5. Results

The geometric accuracy and texture visibility of the final mesh model were evaluated for validation purposes.

In the previous process, the indoor component was scaled to enable the ICP registration (Section 4.2, Step 6). This resulted in alterations to the size of each indoor model, which was the primary focus when discussing the other outcomes of model integration. The report presents the results of scaling each indoor model under the ICP registration, as shown in Table 1. The changes in values before and after the scaling process are shown in Table 2.

The use of relative error (RE) provides a direct and intuitive understanding of the discrepancy between the digital model and the physical object. It is common practice to assess errors in the context of cultural heritage [57]. RE is calculated as the ratio of the absolute difference between the tape measurement and the digital value, relative to the tape measurement. The digital distances in the 3D models were identified using CloudCompare, while the corresponding real-world distances were measured with a tape measure, repeated three times on-site to obtain an average value. In this paper, three distances were selected for each of the six indoor spaces (D1 to D18 in Table 2), and six outdoor distances were selected for the exterior façade and ground of the Mansion (L1 to L6 in Table 3).

Table 1. ICP algorithm scaled report for indoor model registration (scaling values avg.: 0.917).

Indoor Model	Scaling Values	Indoor Model	Scaling Values
Space 1	0.911028	Space 4	0.914089
Space 2	0.911591	Space 5	0.918159
Space 3	0.923556	Space 6	0.922318
Avg.			0.916790

Table 2. Relative error (RE) for 18 distances in indoor spaces (RE% avg.: 7.05% and 3.84%).

Space	Distance	Tape Measure Value (mm)	Digital Value before ICP (mm)	RE %	Digital Value after ICP (mm)	RE %
Space 1	D1	1108	1304 (196)	17.69%	1066 (−42)	3.79%
	D2	2249	----	----	2104 (−145)	6.45%
	D3	1614	1704 (90)	5.58%	1556 (−58)	3.59%
Space 2	D4	1030	1064 (34)	3.30%	975 (−55)	5.34%
	D5	1017	1078 (61)	6.00%	981 (−36)	3.54%
	D6	634	694 (60)	9.46%	631 (−3)	0.47%
Space 3	D7	433	502 (69)	15.94%	461 (28)	6.47%
	D8	704	781 (77)	10.94%	719 (15)	2.13%
	D9	851	906 (55)	6.46%	793 (−58)	6.82%
Space 4	D10	853	833 (−20)	2.34%	796 (−57)	6.68%
	D11	1010	----	----	948 (−62)	6.14%
	D12	793	768 (−25)	3.15%	777 (−16)	2.02%
Space 5	D13	973	1002 (29)	2.98%	957 (−16)	1.64%
	D14	698	733 (35)	5.01%	671 (−27)	3.87%
	D15	473	500 (27)	5.71%	459 (−14)	2.96%
Space 6	D16	1030	1118 (88)	8.54%	1031 (1)	0.10%
	D17	1137	1200 (63)	5.54%	1103 (−34)	2.99%
	D18	710	739 (29)	4.08%	681 (−29)	4.08%
Avg.				7.05%		3.84%

Table 3. Relative error (RE) for six distances in the outdoor environment (RE% avg.: 4.93%).

Distance	Tape Value (mm)	Digital Value (mm)	RE %
L1	420	393 (−24)	6.43%
L2	920	949 (29)	3.15%
L3	2400	2294 (−106)	4.42%
L4	731	682 (−49)	6.70%
L5	718	695 (−23)	3.20%
L6	1460	1377(−83)	5.68%
Avg.			4.93%

In the context of texture visibility within digital models in the heritage domain, rotation is used to facilitate a comparison between images captured at the same angle as those obtained through on-site photography [57], as shown in Figure 7. Additionally, the integration of indoor and outdoor models is a crucial area of examination, with an evaluation of texture visibility in this region necessary to assess the degree of smoothness and comfort in the transition, as shown in Figures 8 and 9.



Figure 7. Comparison of real images (**left**) and corresponding 3D model (**right**).



Figure 8. Enlargement of spatial joints of the ground floor (**top**) and the first floor (**bottom**).

The 'doming effect' refers to a large-scale, systematic deformation of the reconstructed terrain surface, commonly observed in SfM photogrammetry and results from inaccuracies in modeling the radial distortion of the camera lens. Identifying it in the reconstruction of walls, ceilings, and floors is crucial [37]. This allows for the assessment of whether surfaces intended to be vertical or horizontal exhibit irregularities such as bumpiness or mottling [5]. To achieve this, clutter, such as decorations with visible concave and convex variations covering the flat surfaces, was segmented, leaving behind only the relevant areas. A plane was constructed using the random sampling and consensus (RANSAC) algorithm in CloudCompare, which calculates the necessary parameters to construct a corresponding primitive from a minimum set of points. This plane was then fitted to the

remaining parts, accurately representing the flat areas. The distance between each point and the fitted plane was calculated to quantify the degree of the doming effect [36]. In this study, six surfaces from the outdoor environment and three planes from each of the six indoor spaces of the Mansion were selected to represent the ceilings, walls, and floors. A total of 24 surfaces were selected, representing both indoor and outdoor spaces. The results of the calculations are presented in Figures 10 and 11, showing the root mean square error (RMSE) of the distance between each point and the fitted plane, along with the statistical plots, respectively.



Figure 9. Axonometric views of the profile along the y-axis.

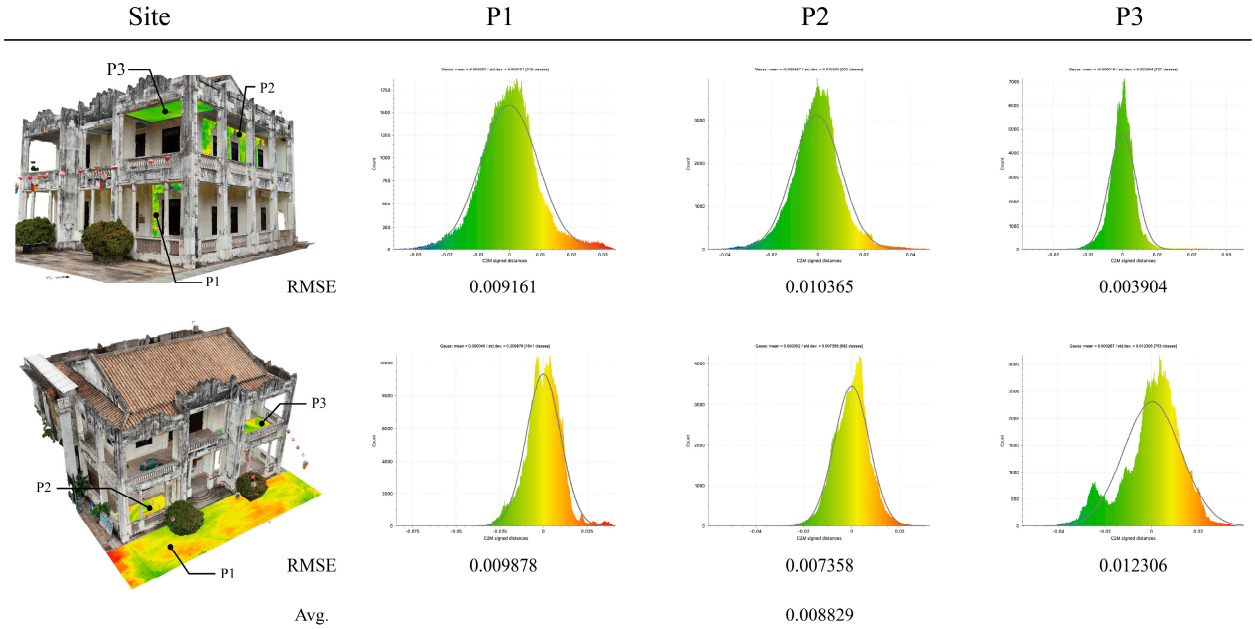


Figure 10. Results of the doming effect in the outdoor environment.

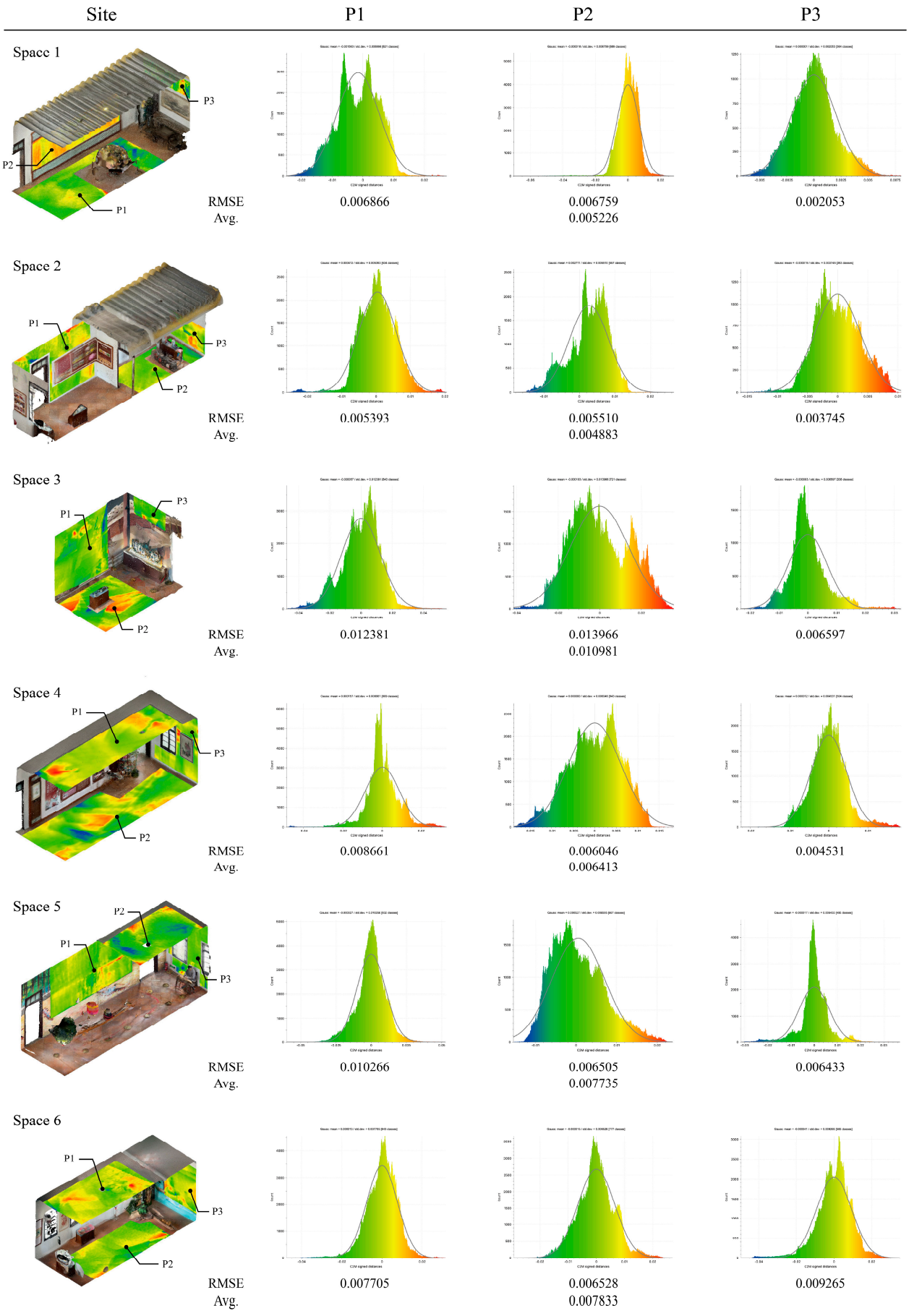


Figure 11. Results of the doming effect in indoor spaces.

6. Discussion

6.1. Drift Error

Table 1 shows that the model exhibited an indoor scaling factor of 0.91679 after ICP registration. This suggests that the indoor models scanned with the iPhone-LiDAR were, on average, scaled down by 9.33%. This observed value can be attributed to a drift error, which caused the digital model to be larger than the real one [35].

As shown in Table 2, 18 indoor planar distances were selected for analysis. However, distances D2 and D11 were excluded due to incorrect texture mapping, which prevented the selection of their endpoints. As a result, only 16 valid planar distances remained. The results showed that the RE decreased after the ICP scaling process, with the mean RE reduced from 7.05% to 3.84%. The largest reduction in RE occurred in D1, with a decrease of 13.9%. Similarly, distances D7, D6, D8, and D16 exhibited decreases of over 8%, with RE reductions of 9.47%, 8.99%, 8.81%, and 8.45%, respectively. For these distances, most of the points, except for D8, were located at the end of the iPhone scanning path, where drift errors were observed, as noted in previous studies [35,52]. This discrepancy may result from an offset in the actual space, caused by deviations in the iPhone's sensors from the recorded scanning path [35]. Nevertheless, Figure 8 shows that the alignment of the indoor and outdoor data improved through scaling.

In summary, the 'scaled' ICP algorithm can be considered a 'correction', specifically the drift error in the iPhone-LiDAR that indoor models can address through precise registration in the WGS84 geographic coordinate system. This approach is similar to optimizing the absolute accuracy of drone photogrammetry using GCPs. This demonstrates that the use of tools with GNSS capabilities can effectively address the issue of drift error in the iPhone scanning model. These results are consistent with the findings in reference [52], which employed a total station optimization method.

6.2. Relative Error

The data comparison and statistics for the 24 distances used to assess the RE of the 3D digital model are presented in Tables 2 and 3.

The RE of the outdoor part of the model was controlled within 6.7%, with an average of 4.93%, as shown in Table 3. This indicates a higher level of accuracy in the outdoor geometry of the experiment compared to previous results using similarly sized and weighted microdrones. This improvement is likely due, on the one hand, to the more advanced GNSS sensor on the DJI Mini 4 Pro, and, on the other hand, to the enhanced SfM photogrammetry algorithm in Metashape Pro, which was refined for image recognition through software development. Advances in both hardware and software have collectively improved the precision of 3D documentation in architectural heritage.

On the right side of Table 2, the mean RE of the indoor area was 3.84%, with a maximum of 6.82% observed in D9 of Space 3 and a minimum of 0.10% in D16 of Space 6. Space 5 exhibited the best performance for the indoor area, with the RE distribution of the three distances being more stable and a maximum RE of 3.87%. However, the distribution of the three distances for Space 2 fluctuated significantly, likely due to the partitioning of the space by a wall (Figure 3), which made the scanning process more challenging and caused data fluctuations. This considerable variation may stem from the partitioning of the indoor space by a wall, adding complexity to the scanning process and causing data fluctuations. When a similar space is encountered, it may be beneficial to divide the area into multiple scans by using the wall as a demarcation point.

Compared to the 10 cm error identified in previous assessments of scanning model accuracy [22,29,36], the significant reduction in error for the indoor portion could be due to the precise registration and 'correction' of drift error (Section 6.1) achieved through

the integration of DJI Mini 4 Pro data. This approach provides a more cost-effective and efficient alternative to the instrumental accuracy of TLS.

The optimization of the Mansion's digital 3D model showed a mean RE of 4.93%, as presented in Tables 2 and 3, indicating an error of approximately 5 cm within a 1-m range. Compared to the conventional combination of TLSs and PMDs, the proposed EDC scheme is not suitable for research requiring millimeter-level accuracy such as restoration applications and structural analyses. Instead, it provides a cost-effective and portable preliminary assessment, ideal for identifying potential issues in the early stages of a project or conducting broader analyses of building-related information.

6.3. Texture Visibility

Figures 7 and 8 show the 3D model with realistic texture reproduction, free from issues like pulling or ghosting. Additionally, viewers could easily identify the materials of the geometric objects in the Mansion. This indicates that the mapping was complete for both the indoor and outdoor sections. Figure 9 presents the axonometric maps of the model, intersecting at the y-axis, which were used to assess the internal and external spatial texture correspondence, transitions, and the integrity of the integrated model. It is clear that the spatial reconstruction of the model was complete, with corresponding texture mapping in each section.

The intersections between each space of the mesh model were then selected, zoomed in for detailed inspection, and exported for orthographic evaluation, as shown on the right side of Figure 8. To demonstrate the benefits of the optimized workflow, a comparison with the unoptimized model of the same site is presented, as shown in Figure 12.

In Figure 12a, the individual spatial models exported by the 3D Scanner App and the outdoor models generated by SfM photogrammetry exhibited a significant discrepancy in color tone between the textures of the same ground area. When the model was rigidly aligned, it created a visual obstruction when navigating between the indoor and outdoor spaces, which is an issue that must be addressed in the digital representation of cultural heritage. This issue arose from using two distinct types of EDC equipment, which generated the digital models: texture mapping and the referencing of images captured by the iPhone 15 Pro indoors and the DJI Mini 4 Pro outdoors. These processes were influenced by objective factors including color sensors, photography algorithms, and light source adaptation, which varied between the indoor and outdoor settings. Consequently, discrepancies in hue appeared between the images captured in each part, and the reconstruction of each part did not consistently reference the corresponding images.

As shown in Figure 12b, only SfM photogrammetry was used for the digital reconstruction of the Mansion, as described in the first five steps of Section 4.2, without replacing the iPhone-LiDAR scanning model. The result was a seamless transition of texture mapping at the intersection; however, the doming effect on the ground and walls on both sides became more pronounced, reducing the visibility of the digital model. This discrepancy, however, did not appear to impact the visibility as significantly as the rigid alignment.

In Figure 12c, the 3D model optimized through the workflow showed a smooth texture when viewed up close, with the doming effect further reduced. In conclusion, the optimized model demonstrated the advantages of LiDAR scanning and SfM photogrammetry, as evidenced by the flat grid and smooth texture transitions at the indoor–outdoor interface. This 3D documentation approach can be applied to digital visualizations of architectural heritage.

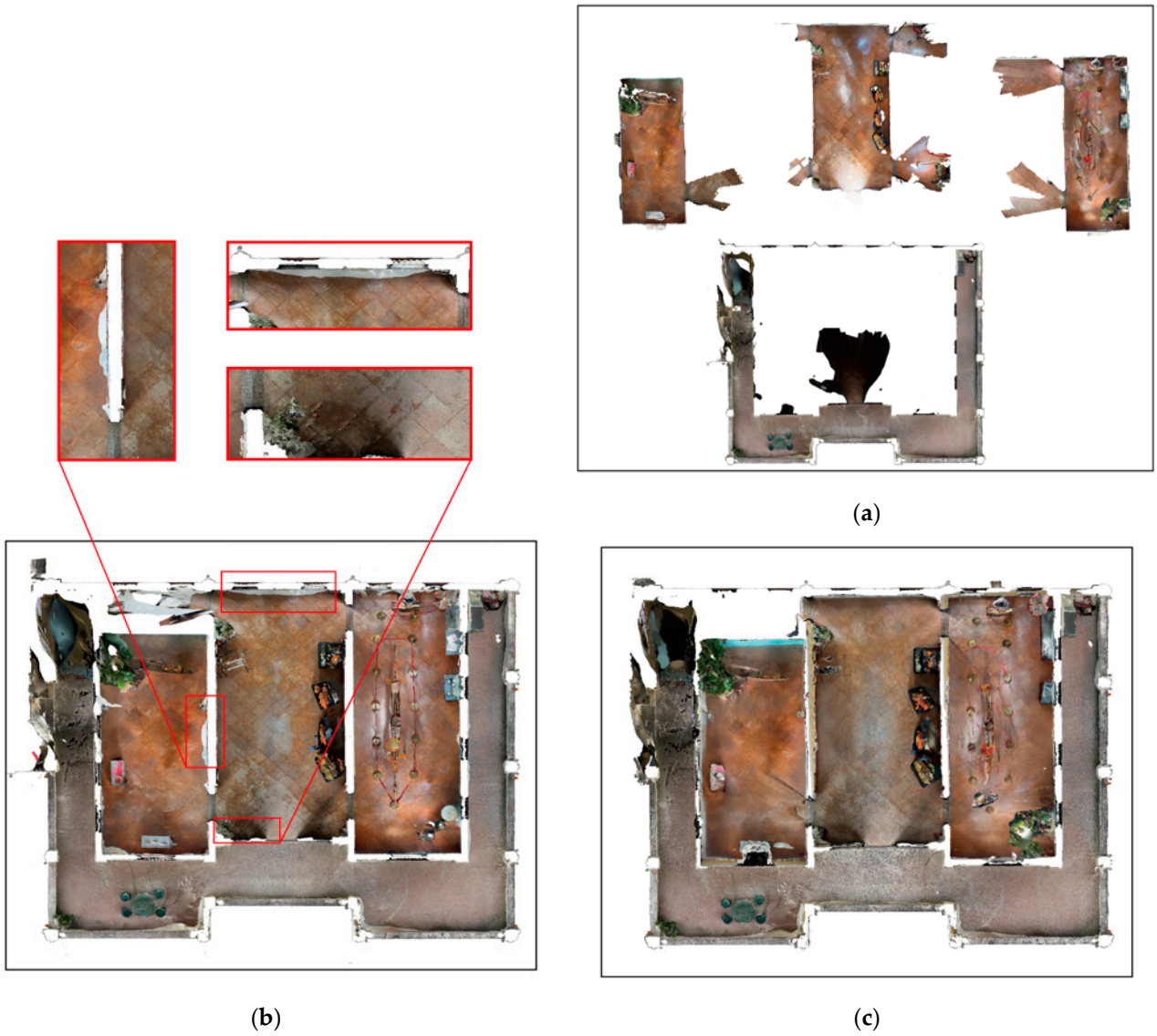


Figure 12. Comparison of the first floor plan models generated by three methods: (**a**) 3D model of each space exported using different technologies; (**b**) 3D model generated using SfM photogrammetry only; (**c**) 3D model with optimization method applied.

6.4. Doming Effect

As shown in Figure 10, the Gaussian distributions of the six selected outdoor components followed a normal distribution, indicating that the mesh discretization for the outdoor surfaces was stable. The maximum RMSE was 0.012306 m, the minimum value was 0.003904 m, and the average was approximately 0.008829 m. The results demonstrate that the reconstruction of the wall and floor components of the outdoor sections, generated by SfM photogrammetry, had been effectively restored, exhibiting the desired doming effect, with average discretization values of 8.9 mm.

For the indoor component, the ceiling, floor, and vertical walls of the medium model were selected for validation. As shown in Figure 11, the statistical graph showed that the maximum RMSE value was 0.010981 m for Space 3, and the minimum value was 0.004883 m for Space 2, based on the selected validation portion for each indoor space. As illustrated in the effect graph on the right side of Figure 11, the statistical graphs for the various parts of the model followed a normal distribution, indicating that the spatial frame of the indoor part of the model was accurate. The mean RMSE for all interior spaces was found to be less than 1 cm, except for Space 3. The P2 portion of Space 3, specifically the

ground, exhibited the highest RMSE value. The analysis of Figure 8 showed that the texture in this section exhibited slight re-shading due to significant changes in light and shadow during data collection (which highlights the importance of rapid acquisition, as discussed in Section 3.3), resulting in a more pronounced doming effect in this space compared to the other five.

Figure 13 compares the optimized model with the only SfM photogrammetry model of the same indoor spaces to demonstrate the advantages of the optimized workflow. The unoptimized model exhibited a particularly pronounced doming effect, especially on the ceiling. This finding supports previous studies that indicate that LiDAR scanning reconstruction is more effective than SfM photogrammetry for constructing spatial frameworks in indoor models. The results confirm that the optimization method presented in this paper fully leverages the strengths of iPhone-LiDAR in constructing indoor space frames, thereby reducing the doming effect. At the same time, the method preserves the superior texture mapping capabilities of SfM photogrammetry, effectively addressing the texture mismatch in iPhone-LiDAR.

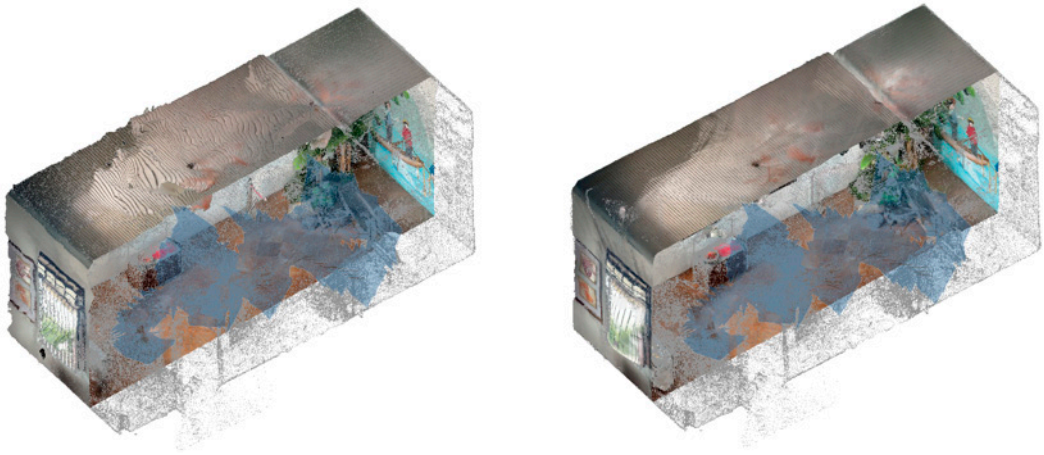


Figure 13. Comparison of only SfM photogrammetry model (**left**) and optimized model (**right**).

7. Conclusions

This paper investigated the potential of EDC equipment as a portable, low-cost, and efficient tool for rapid 3D digital documentation. To evaluate whether traditional TLSs and PMDs could be replaced by a low-cost solution, two EDC devices were utilized: a LiDAR-equipped mobile phone (iPhone 15 Pro) and an under 250 g microdrone (DJI Mini 4 Pro). Additionally, the objective was to produce 'archive-grade' 3D digital documentation [5]. Going back to the goals (low-cost, portable, precise and visibility) of the research the following conclusions were made:

1. Models generated using iPhone-LiDAR are prone to drift errors; however, these can be corrected by adjusting the coordinate system in the SfM photogrammetry reconstruction to align with the scaling.
2. In the optimized workflow, iPhone-LiDAR scanning reduces the doming effect in SfM photogrammetry for indoor spaces, while combining SfM photogrammetry with a microdrone corrects the drift error and texture mapping mismatch of iPhone-LiDAR. The iPhone and microdrone complement each other's limitations and enhance their respective strengths.
3. Unlike previous studies, which only enabled qualitative investigations and visualizations of the microdrone data, the 3D model generated by the optimization scheme allows for quantitative analysis with centimeter-level accuracy.

4. The optimized 3D model presented can be used for digital presentations of architectural heritage, offering an excellent visualization of the integrated outdoor and indoor textures, as shown in Figures 7–9. This is particularly important in fields like cultural heritage, where digital models are often required for presentation.

However, the proposed method still has some limitations in balancing the cost and portability of the device:

1. The glass cover of the collection was unable to be fully reconstructed, despite the use of iPhone-LiDAR and SfM photogrammetry. The highly reflective nature of these objects continues to present a significant challenge for 3D documentation, however, this issue can be addressed through subsequent model corrections.
2. The resolution of the image dataset exported from the 3D Scanner App was insufficient to match the pixel resolution of the iPhone camera, resulting in poorly defined texture maps in the indoor section. To address this issue, additional indoor image datasets can be captured using a camera. It is expected that future versions of the application will resolve this limitation.
3. The optimization method is only applicable to devices with a LiDAR sensor on the iOS platform, as only 3D documentation applications on this platform can access the LiDAR sensor. However, mobile devices equipped with LiDAR are not confined to the iOS platform, and it is expected that more applications will be adapted for other platforms.
4. The geometric accuracy of the final model greatly depends on the precision of the microdrones' onboard GPS, which is significantly influenced by environmental factors such as signal strength and terrain characteristics. If the budget permits, a compact ground station integrated with GCPs can be used to enhance the geometric accuracy of the data, providing a more precise solution.

Table 4 provides a visual comparison of the advantages and disadvantages of the most widely used 3D documentation techniques and the proposed method.

Table 4. A comparison of the widely used 3D documentation methods and the proposed method.

	Widely Used Methods		**Proposed Method**	
Equipment	TLS	PMD	iPhone + Gimbal	Microdrone
Price	>$50,000	>$10,000	$999 + $139	$1099
Weight	>15,000 g		1475 g	
Techniques	Range-based	Image-based	SLAM	Image-based
Data integration	Same CGPs matching		Optimal workflow	
Geometric accuracy	Millimeter-level		Centimeter-level	
Texture visibility	Rigid		Smooth	

It should be noted that the table does not specify which method corresponds to each objective. As discussed in the introduction, it is essential to orient the use of each method and instrument toward clearly defined results. Furthermore, to develop a feasible approach, factors such as available financial resources, the environmental context of the site, and local drone flight restrictions must be considered. However, we tried to envision suitable users and use cases for the proposed method based on its characteristics.

The proposed method is ideal for beginners and amateurs in the heritage field, as the low-cost, portable EDC equipment features can assist them in efficiently creating a 3D documentation of heritage sites. Additionally, when experts face a large number of existing or 'minor' heritage sites, such as the Mansion, the proposed method enables the rapid creation of a comprehensive digital archive. This process can contribute to the democratization of cultural heritage, as discussed in [36,38], and facilitate the documentation

of more architectural heritage sites. In the context of digitally displaying architectural heritage, the need for visualization often outweighs the need for precision. The proposed method produces a superior 3D digital model with enhanced visual appeal and integrated indoor and outdoor spaces. It can also promote education and public participation in cultural heritage.

The proposed method is also well-suited for investigating cultural routes with high heritage density, where equipment weight is a key consideration. A microdrone weighing under 250 g can easily take-off in most countries without restrictions, ensuring smooth research progression, even when crossing international borders. Additionally, for larger heritage sites (e.g., historical towns or villages), microdrones can be used for flight planning to capture oblique photographs, enabling the creation of large-scale 3D models. These can then collect outdoor data through close-range photography for individual buildings requiring detailed mapping, while the iPhone can scan the indoor spaces. The datasets from both devices can be integrated using the proposed method to produce a comprehensive 'rough with details' model of the heritage site. In the future, it could support smart city development such as urban environment monitoring.

This method is limited by factors such as equipment cost, weight, and precision, which must be fully considered to ensure its appropriate application under specific conditions; recognizing these limitations is the key to using this method correctly. However, the current development of low-cost LiDAR devices and portable microdrones indicates that these technologies are still evolving. Furthermore, the use of EDC equipment for mapping has not only become a reality, but is also expected to result in improvements in accuracy, cost reductions, and increased portability in the foreseeable future. This further emphasizes the application and importance of this method. The evolution of low-cost sensors may facilitate the future integration of LiDAR sensors on microdrones, which could then be employed in conjunction with the methodology outlined in this paper to replace the entire building model, rather than just the interior components. This approach could yield more precise architectural heritage 3D digital documentation through EDC equipment.

Author Contributions: Conceptualization, N.Z. and X.L.; Methodology, X.L.; Software, N.Z.; Validation, X.L.; Formal analysis, N.Z.; Investigation, X.L.; Resources, X.L.; Data curation, X.L.; Writing—original draft preparation, N.Z. and X.L.; Writing—review and editing, N.Z. and X.L.; Visualization, N.Z.; Supervision, X.L.; Project administration, N.Z. and X.L.; Funding acquisition, N.Z. and X.L. All authors have read and agreed to the published version of the manuscript.

Funding: This research received no external funding.

Data Availability Statement: The original contributions presented in the study are included in the article, further inquiries can be directed to the corresponding authors.

Acknowledgments: We would like to thank Minghao Gao from Huaqiao University for providing the DJI Mini 4 Pro and Yu Fan from Tianjin Chengjian University for providing the DJI Osmo Mobile 6 for this research.

Conflicts of Interest: The authors declare no conflicts of interest.

References

1. Martínez-Carricondo, P.; Carvajal-Ramírez, F.; Yero-Paneque, L.; Agüera-Vega, F. Combination of HBIM and UAV Photogrammetry for Modelling and Documentation of Forgotten Heritage. Case Study: Isabel II Dam in Níjar (Almería, Spain). *Herit. Sci.* **2021**, *9*, 95. [CrossRef]
2. El-Hakim, S.F.; Beraldin, J.; Picard, M.; Godin, G. Detailed 3D reconstruction of large-scale heritage sites with integrated techniques. *IEEE Comput. Graph. Appl.* **2004**, *24*, 21–29. [CrossRef] [PubMed]

3. Tysiac, P.; Sieńska, A.; Tarnowska, M.; Kedziorski, P.; Jagoda, M. Combination of Terrestrial Laser Scanning and UAV Photogrammetry for 3D Modelling and Degradation Assessment of Heritage Building Based on a Lighting Analysis: Case Study—St. Adalbert Church in Gdansk, Poland. *Herit. Sci.* **2023**, *11*, 53. [CrossRef]
4. Remondino, F. Heritage Recording and 3D Modeling with Photogrammetry and 3D Scanning. *Remote Sens.* **2011**, *3*, 1104–1138. [CrossRef]
5. Dostal, C.; Yamafune, K. Photogrammetric Texture Mapping: A Method for Increasing the Fidelity of 3D Models of Cultural Heritage Materials. *J. Archaeol. Sci. Rep.* **2018**, *18*, 430–436. [CrossRef]
6. Murtiyoso, A.; Grussenmeyer, P.; Suwardhi, D. Technical Considerations in Low-Cost Heritage Documentation. *Int. Arch. Photogramm. Remote Sens. Spat. Inf. Sci.* **2019**, *XLII-2/W17*, 225–232. [CrossRef]
7. Nebel, S.; Beege, M.; Schneider, S.; Rey, G.D. A Review of Photogrammetry and Photorealistic 3D Models in Education from a Psychological Perspective. *Front. Educ.* **2020**, *5*, 144. [CrossRef]
8. Polo, M.-E.; Felicísimo, Á.M.; Durán-Domínguez, G. Accurate 3D Models in Both Geometry and Texture: An Archaeological Application. *Digit. Appl. Archaeol. Cult. Herit.* **2022**, *27*, e00248. [CrossRef]
9. Galeazzi, F. 3D recording, documentation and management of cultural heritage. *Int. J. Herit. Stud.* **2017**, *23*, 671–673. [CrossRef]
10. Zhou, W.; Fu, X.; Deng, Y.; Yan, J.; Zhou, J.; Liu, P. The Extraction of Roof Feature Lines of Traditional Chinese Village Buildings Based on UAV Dense Matching Point Clouds. *Buildings* **2024**, *14*, 1180. [CrossRef]
11. Salagean-Mohora, I.; Anghel, A.A.; Frigura-Iliasa, F.M. Photogrammetry as a Digital Tool for Joining Heritage Documentation in Architectural Education and Professional Practice. *Buildings* **2023**, *13*, 319. [CrossRef]
12. Kersten, T.; Mechelke, K.; Maziull, L. 3D Model of AL Zubarah Fortress in Qatar–Terrestrial Laser Scanning vs. Dense Image Matching. *Int. Arch. Photogramm. Remote Sens. Spat. Inf. Sci.* **2015**, *XL-5/W4*, 1–8. [CrossRef]
13. Guo, M.; Sun, M.; Pan, D.; Wang, G.; Zhou, Y.; Yan, B.; Fu, Z. High-Precision Deformation Analysis of Yingxian Wooden Pagoda Based on UAV Image and Terrestrial LiDAR Point Cloud. *Herit. Sci.* **2023**, *11*, 1. [CrossRef]
14. Jaber, A.S.; Abed, F.M. Revealing the Potentials of 3D Modelling Techniques; a Comparison Study towards Data Fusion from Hybrid Sensors. *IOP Conf. Ser. Mater. Sci. Eng.* **2020**, *737*, 012230. [CrossRef]
15. Pepe, M.; Ackermann, S.; Fregonese, L.; Achille, C. 3D Point Cloud Model Color Adjustment by Combining Terrestrial Laser Scanner and Close Range Photogrammetry Datasets. *Int. J. Comput. Inf. Eng.* **2016**, *10*, 1942–1948.
16. Rolin, R.; Antaluca, E.; Batoz, J.-L.; Lamarque, F.; Lejeune, M. From Point Cloud Data to Structural Analysis Through a Geometrical hBIM-Oriented Model. *J. Comput. Cult. Herit.* **2019**, *12*, 1–26. [CrossRef]
17. Yu, R.; Li, P.; Shan, J.; Zhu, H. Structural State Estimation of Earthquake-Damaged Building Structures by Using UAV Photogrammetry and Point Cloud Segmentation. *Measurement* **2022**, *202*, 111858. [CrossRef]
18. Moon, D.; Chung, S.; Kwon, S.; Seo, J.; Shin, J. Comparison and Utilization of Point Cloud Generated from Photogrammetry and Laser Scanning: 3D World Model for Smart Heavy Equipment Planning. *Autom. Constr.* **2019**, *98*, 322–331. [CrossRef]
19. Corradetti, A.; Seers, T.; Mercuri, M.; Calligaris, C.; Busetti, A.; Zini, L. Benchmarking Different SfM-MVS Photogrammetric and iOS LiDAR Acquisition Methods for the Digital Preservation of a Short-Lived Excavation: A Case Study from an Area of Sinkhole Related Subsidence. *Remote Sens.* **2022**, *14*, 5187. [CrossRef]
20. Barsanti, S.G.; Remondino, F.; Fenández-Palacios, B.J.; Visintini, D. Critical Factors and Guidelines for 3D Surveying and Modelling in Cultural Heritage. *Int. J. Herit. Digit. Era* **2014**, *3*, 141–158. [CrossRef]
21. Martínez-Carricondo, P.; Agüera-Vega, F.; Carvajal-Ramírez, F. Use of UAV-Photogrammetry for Quasi-Vertical Wall Surveying. *Remote Sens.* **2020**, *12*, 2221. [CrossRef]
22. Mokroš, M.; Mikita, T.; Singh, A.; Tomaštík, J.; Chudá, J.; Wężyk, P.; Kuželka, K.; Surový, P.; Klimánek, M.; Zięba-Kulawik, K.; et al. Novel Low-Cost Mobile Mapping Systems for Forest Inventories as Terrestrial Laser Scanning Alternatives. *Int. J. Appl. Earth Obs. Geoinf.* **2021**, *104*, 102512. [CrossRef]
23. Tatsumi, S.; Yamaguchi, K.; Furuya, N. ForestScanner: A Mobile Application for Measuring and Mapping Trees with LiDAR-equipped iPhone and iPad. *Methods Ecol. Evol.* **2022**, *14*, 1603–1609. [CrossRef]
24. Balado, J.; Garozzo, R.; Winiwarter, L.; Tilon, S. A Systematic Literature Review of Low-Cost 3D Mapping Solutions. *Inf. Fusion.* **2025**, *114*, 102656. [CrossRef]
25. Ngo, K.H.; Tran, Q.K.; Quan, C.H.; Luu, N.K.N.; Nguyen, M.C.; Dautremont, M.; Badie, A. Photogrammetry-Based Building Scan Using Ultra-Lightweight Drone for Urban Applications. In *Lecture Notes in Civil Engineering*; Springer Nature: Singapore, 2023; pp. 1700–1709. [CrossRef]
26. McGlade, J.; Wallace, L.; Hally, B.; Reinke, K.; Jones, S. The Effect of Surrounding Vegetation on Basal Stem Measurements Acquired Using Low-Cost Depth Sensors in Urban and Native Forest Environments. *Sensors* **2023**, *23*, 3933. [CrossRef] [PubMed]
27. Ulvi, A. Documentation, Three-Dimensional (3D) Modelling and visualization of cultural heritage by using Unmanned Aerial Vehicle (UAV) photogrammetry and terrestrial laser scanners. *Int. J. Remote Sens.* **2021**, *42*, 1994–2021. [CrossRef]
28. Bakirman, T.; Bayram, B.; Akpinar, B.; Karabulut, M.F.; Bayrak, O.C.; Yigitoglu, A.; Seker, D.Z. Implementation of Ultra-Light UAV Systems for Cultural Heritage Documentation. *J. Cult. Herit.* **2020**, *44*, 174–184. [CrossRef]

29. Díaz-Vilariño, L.; Tran, H.; Frías, E.; Balado, J.; Khoshelham, K. 3D Mapping of Indoor and Outdoor Environments Using Apple Smart Devices. *Int. Arch. Photogramm. Remote Sens. Spat. Inf. Sci.* **2022**, *XLIII-B4-2022*, 303–308. [CrossRef]
30. Qiu, Z.; Martínez-Sánchez, J.; Brea, V.M.; López, P.; Arias, P. Low-cost mobile mapping system solution for traffic sign segmentation using Azure Kinect. *Int. J. Appl. Earth Obs. Geoinf.* **2020**, *112*, 102895. [CrossRef]
31. Schops, T.; Sattler, T.; Hane, C.; Pollefeys, M. 3D Modeling on the Go: Interactive 3D Reconstruction of Large-Scale Scenes on Mobile Devices. In Proceedings of the International Conference on 3D Vision, Lyon, France, 19–22 October 2015; pp. 291–299. [CrossRef]
32. Luetzenburg, G.; Kroon, A.; Bjørk, A.A. Evaluation of the Apple iPhone 12 Pro LiDAR for an Application in Geosciences. *Sci. Rep.* **2021**, *11*, 22221. [CrossRef]
33. Cabezos-Bernal, P.M.; Rodríguez-Navarro, P.; Gil-Piqueras, T.; Ribera, M.G. Using Drones under 250 g for Documenting Architectural Heritage. *Disegnarecon* **2022**, *15*, 1–19. [CrossRef]
34. Luetzenburg, G.; Kroon, A.; Kjeldsen, K.K.; Splinter, K.D.; Bjørk, A.A. High-Resolution Topographic Surveying and Change Detection with the iPhone LiDAR. *Nat. Protoc.* **2024**, *19*, 3520–3541. [CrossRef] [PubMed]
35. Teppati Losè, L.; Spreafico, A.; Chiabrando, F.; Giulio Tonolo, F. Apple LiDAR Sensor for 3D Surveying: Tests and Results in the Cultural Heritage Domain. *Remote Sens.* **2022**, *14*, 4157. [CrossRef]
36. Askar, C.; Sternberg, H. Use of Smartphone Lidar Technology for Low-Cost 3D Building Documentation with iPhone 13 Pro: A Comparative Analysis of Mobile Scanning Applications. *Geomatics* **2023**, *3*, 563–579. [CrossRef]
37. Aljadire, A.A.; Khalaf, Y.H. A Study in Preserving Cultural Heritage Using Portable Laser Devices Embedded in Mobile Phones. *IOP Conf. Ser. Earth Environ. Sci.* **2024**, *1374*, 012041. [CrossRef]
38. Murtiyoso, A.; Grussenmeyer, P.; Landes, T.; Macher, H. First Assessments into the Use of Commercial-Grade Solid State Lidar for Low Cost Heritage Documentation. *Int. Arch. Photogramm. Remote Sens. Spat. Inf. Sci.* **2021**, *XLIII-B2-2021*, 599–604. [CrossRef]
39. Çakir, G.Y.; Post, C.J.; Mikhailova, E.A.; Schlautman, M.A. 3D LiDAR Scanning of Urban Forest Structure Using a Consumer Tablet. *Urban Sci.* **2021**, *5*, 88. [CrossRef]
40. Rutkowski, W.; Lipecki, T. Use of the iPhone 13 Pro LiDAR Scanner for Inspection and Measurement in the Mineshaft Sinking Process. *Remote Sens.* **2023**, *15*, 5089. [CrossRef]
41. Gentili, F.; Madonna, S. Photogrammetry from UAV and Low-Cost Lidar for Sinkhole Hazard Mitigation in Urban Areas: Applications and Evaluations. *Geographies* **2024**, *4*, 343–362. [CrossRef]
42. Kottner, S.; Thali, M.J.; Gascho, D. Using the iPhone's LiDAR Technology to Capture 3D Forensic Data at Crime and Crash Scenes. *Forensic Imaging* **2023**, *32*, 200535. [CrossRef]
43. King, F.; Kelly, R.; Fletcher, C.G. New opportunities for low-cost LiDAR-derived snow depth estimates from a consumer drones-mounted smartphone. *Cold Reg. Sci. Technol.* **2023**, *207*, 103757. [CrossRef]
44. Tamimi, R.; Toth, C. Performance Assessment of a Mini Mobile Mapping System: Iphone 14 pro Installed on a e-Scooter. *Int. Arch. Photogramm. Remote Sens. Spat. Inf. Sci.* **2023**, *XLVIII-M-3–2023*, 307–315. [CrossRef]
45. Günen, M.A.; Erkan, İ.; Aliyazicioğlu, Ş.; Kumaş, C. Investigation of Geometric Object and Indoor Mapping Capacity of Apple iPhone 12 Pro LiDAR. *Mersin Photogramm. J.* **2023**, *5*, 82–89. [CrossRef]
46. Tamimi, R.; Toth, C. Experiments with Combining LiDAR and Camera Data Acquired by UAS and Smartphone to Support Mapping. *Int. Arch. Photogramm. Remote Sens. Spat. Inf. Sci.* **2024**, *XLVIII-1–2024*, 619–627. [CrossRef]
47. Gopal, L.; Shukor, S.A.A. Modelling Small Artefact for Preservation—A Case Study of Perlis Heritage. *J. Phys. Conf. Ser.* **2023**, *2641*, 012005. [CrossRef]
48. Dörtbudak, B.; Akca, S. Investigating the Utilization of iPhone LiDAR Sensor in Documenting Cultural Heritage. *Intercont. Geoinf. Days (IGD)* **2023**, *7*, 217–221.
49. Voûte, R.L.; Prins, H.; Smit, B.-P. Comparison of Low-Cost Techniques for Digital Cultural Heritage Preservation of an Original Egyptian Temple. *AGILE GIScience Ser.* **2023**, *4*, 49. [CrossRef]
50. Jakovljević, G.; Govedarica, M.; Alvarez Taboada, F. Iphone 13 Pro vs. Professional TLS for 3D Indoor Mapping. *Stepgrad* **2021**, *15*, 274–282. [CrossRef]
51. University, P.M.; Suranov, N.A.; Romanchikov, A.Y.; Valkov, V.A. The Examination of a Possibility for Usage of an Iphone 12 Pro Lidar to Indoor Measurements for State Cadastral Registration. *Vestnik SSUGT* **2023**, *28*, 33–46. [CrossRef]
52. Tamimi, R. Relative Accuracy Found within Iphone Data Collection. *Int. Arch. Photogramm. Remote Sens. Spat. Inf. Sci.* **2022**, *XLIII-B2-2022*, 303–308. [CrossRef]
53. Barbosa, P.C.; Fargas, D.C., Jr.; Narciso, G.A.M. Comparative Analysis of Low-Cost Consumer-Grade and Commercial-Grade Drones for Land Surveying Applications. *Int. Arch. Photogramm. Remote Sens. Spat. Inf. Sci.* **2024**, *XLVIII-4/W8-2023*, 31–37. [CrossRef]
54. Adami, A.; Fregonese, L.; Gallo, M.; Helder, J.; Pepe, M.; Treccani, D. Ultra Light Uav Systems for the Metrical Documentation of Cultural Heritage: Applications for Architecture and Archaeology. *Int. Arch. Photogramm. Remote Sens. Spat. Inf. Sci.* **2019**, *XLII-2/W17*, 15–21. [CrossRef]

55. Bedford, J. *Photogrammetric Applications for Cultural Heritage*; Historic England: Swindon, UK, 2017; p. 27.x.
56. Tondo, G.R.; Riley, C.; Morgenthal, G. Characterization of the iPhone LiDAR-Based Sensing System for Vibration Measurement and Modal Analysis. *Sensors* **2023**, *23*, 7832. [CrossRef] [PubMed]
57. Jalandoni, A.; Domingo, I.; Taçon, P.S.C. Testing the Value of Low-Cost Structure-from-Motion (SfM) Photogrammetry for Metric and Visual Analysis of Rock Art. *J. Archaeol. Sci. Rep.* **2018**, *17*, 605–616. [CrossRef]

Disclaimer/Publisher's Note: The statements, opinions and data contained in all publications are solely those of the individual author(s) and contributor(s) and not of MDPI and/or the editor(s). MDPI and/or the editor(s) disclaim responsibility for any injury to people or property resulting from any ideas, methods, instructions or products referred to in the content.